Electronic Properties of Graphene Multilayers

Johan Nilsson,[1] A. H. Castro Neto,[1] F. Guinea,[2] and N. M. R. Peres[3]

[1]*Department of Physics, Boston University, 590 Commonwealth Avenue, Boston, Massachusetts 02215, USA*
[2]*Instituto de Ciencia de Materiales de Madrid, CSIC, Cantoblanco E28049 Madrid, Spain*
[3]*Center of Physics and Departamento de Física, Universidade do Minho, P-4710-057, Braga, Portugal*

(Received 11 April 2006; published 26 December 2006)

We study the effects of disorder in the electronic properties of graphene multilayers, with special focus on the bilayer and the infinite stack. At low energies and long wavelengths, the electronic self-energies and density of states exhibit behavior with divergences near half filling. As a consequence, the spectral functions and the conductivities acquire anomalous properties. In particular, we show that the quasiparticle decay rate has a minimum as a function of energy, there is a universal minimum value for the in-plane conductivity of order e^2/h per plane and, unexpectedly, the c-axis conductivity is enhanced by disorder at low doping, leading to an enormous conductivity anisotropy at low temperatures.

DOI: 10.1103/PhysRevLett.97.266801 PACS numbers: 73.21.Ac, 71.23.−k, 81.05.Uw

Introduction.—Recently, many properties of a single graphene sheet have been studied theoretically by several groups. These properties are, in many cases, found to be unconventional due to the peculiar band structure of graphene which is described in terms of Dirac fermions at the edge of the Brillouin zone (BZ). This activity was triggered by the realization that graphene could be obtained and studied experimentally [1], and the subsequent experiments that followed to further characterize the material [2,3].

More recently the attention has turned to graphene multilayers [4] and, in particular, to bilayers that also show anomalies in the integer quantum Hall effect (IQHE) [5] and have received theoretical attention [6,7]. In this paper we show that the graphene bilayer also has very unconventional behavior in its spectral and transport properties. These properties, however, are quite different from those of the single layer. In fact, the anomalous behavior is a property of all multilayer graphene systems we have studied. It is also worth noting that the higher complexity of the multilayer systems may be of interest for device applications since it also allows for greater flexibility in tailoring the electronic properties.

There are two key ingredients that make the physics of the graphene multilayers unconventional. First, due to the relatively weak interlayer coupling it inherits some properties from its parent material, the single graphene sheet. The existence of Dirac points in the BZ, where the electron and hole bands becomes degenerate, arises from the physics of the single layer in conjunction with the second important ingredient that is the peculiar geometry that results from the A-B stacking of the planes. This geometry implies that the binding of the planes due to orbital overlap is mainly sitting on one of the sublattices (that we call A, the other sublattice being B) in each plane (the different planes of the units cell are denoted by 1 and 2). The main residence of the low-energy states is then on the sublattice B. Nevertheless, electron transport coming from nearest neighbor hopping must go over the A sublattice. This feature implies that even though the total density of states at half filling is finite, the density of states on the A sublattice vanishes as the Dirac point is approached, leading to unconventional in-plane and out-of-plane transport properties. The main purpose of this work is to show how this comes about and to highlight the unusual behavior of the self-energies due to disorder near half filling.

Graphene bilayer.—At low energies and long wavelengths, one can expand the electronic spectrum close to the K and K' points in the BZ, leading to a Hamiltonian of the form [8]: $H = \sum_{\mathbf{k}} \Psi^\dagger(\mathbf{k}) \mathcal{H}_0(\mathbf{k}) \Psi(\mathbf{k})$, where $\mathbf{k} = (k_x, k_y)$ is the two-dimensional momentum measured relative to the K (K') point,

$$\mathcal{H}_0(\mathbf{k}) = v_F \begin{pmatrix} 0 & k e^{i\phi(\mathbf{k})} & t_\perp/v_F & 0 \\ k e^{-i\phi(\mathbf{k})} & 0 & 0 & 0 \\ t_\perp/v_F & 0 & 0 & k e^{-i\phi(\mathbf{k})} \\ 0 & 0 & k e^{i\phi(\mathbf{k})} & 0 \end{pmatrix}, \tag{1}$$

$\Psi^\dagger(\mathbf{k}) = (c^\dagger_{A_1,\mathbf{k}} c^\dagger_{B_1,\mathbf{k}} c^\dagger_{A_2,\mathbf{k}} c^\dagger_{B_2,\mathbf{k}})$ is the electron spinor creation operator, $\phi(\mathbf{k}) = \tan^{-1}(k_y/k_x)$ is the two-dimensional angle in momentum space, $v_F = 3ta/2$ is the Fermi-Dirac velocity, $t \approx 3$ eV is the in-plane hopping energy, $a \approx 1.42$ Å is the interatomic distance within the layers, $t_\perp \approx 0.35$ eV is the interlayer hopping energy [9]. The 2×2 blocks on the diagonal of (1) are identical to the continuous approximation that leads to the massless Dirac spectrum in a single layer. In what follows we use units such that $v_F = 1 = \hbar$, and suppress the spin and valley indices unless otherwise specified. The Hamiltonian (1) can be easily diagonalized and the energy spectrum is made out of four bands with energy: $t_\perp/2 \pm E(k)$ and $-t_\perp/2 \pm E(k)$, where $E(k) = \sqrt{t_\perp^2/4 + k^2}$. The resulting spectrum is made out of two vertex touching hyperbolae at zero energy, separated by a gap of energy $t_\perp$ from two other hyperbolas.

In what follows it is convenient to introduce a local frequency-dependent self-energy which, due to the lattice structure, has different values in the A [$\Sigma_A(\omega)$] and the B [$\Sigma_B(\omega)$] sublattices. We take these into account by a diagonal matrix $\mathcal{H}_\Sigma(\omega)$ and the Green's function is then given by

$$G^{-1}(\omega, \mathbf{k}) = \omega - \mathcal{H}_0(\mathbf{k}) - \mathcal{H}_\Sigma(\omega). \tag{2}$$

Because the Hamiltonian factorizes into two blocks it is simple to work out the explicit expression for the Green's function. $G(\omega, \mathbf{k})$ is a 4×4 matrix, but for our purposes here the most important components are the diagonal ones that are given by

$$G^D_{AA}(\omega, k) = \sum_{\alpha=\pm} [\omega - \Sigma_B(\omega)]/[2D_\alpha(\omega, k)],$$
$$G^D_{BB}(\omega, k) = \sum_{\alpha=\pm} [\omega - \Sigma_A(\omega) + \alpha t_\perp]/[2D_\alpha(\omega, k)],$$
$$D_\pm(\omega, k) = [\omega \pm t_\perp - \Sigma_A(\omega)][\omega - \Sigma_B(\omega)] - k^2.$$

Effects of disorder.—We use standard techniques to study the effect of disorder and average over impurity positions to get the disorder-averaged propagators [10]. The effect of repeated scattering from a single impurity can be encoded in a self-energy which can be computed in the T-matrix approximation as

$$\Sigma(\omega) = V[1 - \bar{G}(\omega)V]^{-1}/N, \qquad \bar{G}(\omega) = \sum_{\mathbf{k}} G(\omega, \mathbf{k})/N, \tag{3}$$

where V is the strength of the impurity potential and N is the number of units cells in each plane. We turn the momentum sum into an integral by the introduction of a cut off, Λ ($\approx 1/a$), that we estimate ($\Lambda \approx 7$ eV) by a Debye approximation conserving the number of states in the BZ [7]. Because of the special form of the propagator and the impurity potential, the self-energy is diagonal. The result for unitary scattering (or site dilution) is obtained by introducing a finite density of vacancies n_i and taking the limit $V \to \infty$, and one finds

$$\Sigma_A(\omega) = -n_i/\bar{G}^D_{AA}(\omega), \qquad \Sigma_B(\omega) = -n_i/\bar{G}^D_{BB}(\omega). \tag{4}$$

In the full Born approximation (FBA) one uses the bare propagators on the right-hand side of (4); the resulting self-energies are linear in the impurity concentration so that this approximation neglects all correlations between different scattering centers. In the coherent potential approximation (CPA) [11] one assumes that the electrons are moving in an effective medium that is characterized by the self-energies Σ_A and Σ_B. These must be determined self-consistently by using the dressed propagators on the right-hand side of (4), thus this approximation includes some effects of correlations between the scattering events (it does not describe Anderson localization). Using the explicit form of the propagators we obtain the following self-consistent equations

$$\frac{n_i}{\Sigma_A} = \frac{\omega - \Sigma_B}{2\Lambda^2} \sum_{\alpha=\pm} \ln\left[\frac{\Lambda^2}{-(\omega + \alpha t_\perp - \Sigma_A)(\omega - \Sigma_B)}\right],$$
$$\frac{n_i}{\Sigma_B} = \frac{\omega - \Sigma_A}{2\Lambda^2} \sum_{\alpha=\pm} \ln\left[\frac{\Lambda^2}{-(\omega - \alpha t_\perp - \Sigma_A)(\omega - \Sigma_B)}\right] + \frac{t_\perp}{2\Lambda^2} \ln\left[\frac{-(\omega - t_\perp - \Sigma_A)(\omega - \Sigma_B)}{-(\omega + t_\perp - \Sigma_A)(\omega - \Sigma_B)}\right]. \tag{5}$$

The CPA self-energies depend only on the local propagator (i.e., $\bar{G}$), which at low energies has two equal contributions coming from the two K points. Therefore (5) do include intervalley scattering in the intermediate states, while to perform the calculations one can work near one K point only. It is also straightforward to obtain the density of states (DOS) on sublattice a ($a = A, B$) from $\rho_a(\omega) = -\mathrm{Im}\bar{G}^D_{aa}/\pi$. In the clean case, one gets

$$\rho^0_A(\omega) = |\omega|[1 + \Theta(|\omega| - t_\perp)]/2\Lambda^2,$$
$$\rho^0_B(\omega) = \rho^0_A(\omega) + t_\perp[1 - \Theta(|\omega| - t_\perp)]/2\Lambda^2,$$

where $\Theta(x)$ is the Heaviside step function. Notice that the DOS on the A sublattice vanishes at zero energy (as in the case of a single layer), while $\rho^0_B(0)$ is finite.

We have solved the CPA equations in Eq. (5) and an example of the resulting self-energies and the corresponding DOS are shown in Fig. 1. Within the FBA Σ_A diverges as $n_i\Lambda^2/\omega$ up to logarithmic corrections as $\omega \to 0$. In the single layer, the CPA makes the self-energy finite at $\omega = 0$. In contrast, the bilayer (and the multilayer) does not allow a finite Σ_A at $\omega = 0$ in the CPA. One can see this by studying Eq. (5) at $\omega = 0$. Then the last line of Eq. (5) divided by Σ_A must vanish, and this is not possible for finite values of Σ_A, furthermore Σ_B must vanish in this

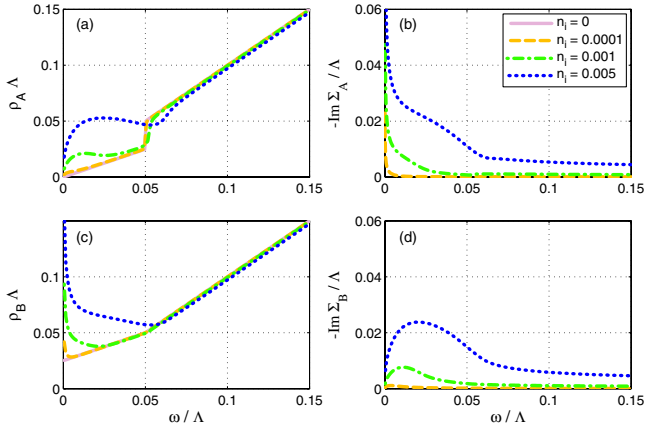

FIG. 1 (color online). Bilayer DOS and self-energy (in units of Λ) in the CPA approximation. DOS on the A (a) and B (c) sublattice as a function of the frequency (in units of Λ), imaginary part of the self-energy on the A (b) and B (d) sublattice as a function of the frequency.

limit. These results imply that, contrary to the single plane case, $\rho_A(\omega \to 0)$ is zero even within the CPA. More explicitly, by defining $\Sigma_A\Sigma_B = -\xi\Lambda^2$ one can show (assuming $\Sigma_A \gg t_\perp$ and $\Sigma_B \gg \omega$) that Σ_A and Σ_B are given asymptotically by

$$\Sigma_A(\omega) \approx e^{-i\pi/3}(t_\perp^2\xi^2\Lambda^2/n_i)^{1/3}\omega^{-1/3}, \quad (6a)$$

$$\Sigma_B(\omega) \approx e^{-i2\pi/3}(n_i\Lambda^4\xi/t_\perp^2)^{1/3}\omega^{1/3}, \quad (6b)$$

for $\omega \ll \Lambda^2\xi^2/n_i t_\perp$, where ξ is given by $n_i = \xi\ln(1/\xi)$. The large frequency dependence of the self-energies is rather unusual. Note that $\sqrt{\xi}\Lambda \sim \sqrt{n_i}\Lambda$ is exactly the scale generated by disorder in the single plane case [10].

Infinite stack.—The extension of the bilayer model to multilayers is straightforward. Upon a Fourier transformation in the c direction we can immediately use the Hamiltonian in Eq. (1) with $\mathbf{k} = (k_x, k_y, k_\perp)$, where $k_\perp$ is the momentum along the c axis ($-\pi/2 < k_\perp d \le \pi/2$), and make the substitution $t_\perp \to 2t_\perp\cos(k_\perp d)$, where $d \approx 2.5a$ is the interlayer distance [8]. The calculations of the DOS and self-energies proceed as previously but with one additional $k_\perp$ integral [12]. The electron spectral function, that is measurable in angle resolved photoemission (ARPES), is given by

$$A(\mathbf{k}, \omega) = -(2/\pi)\mathrm{Im}[G^D_{AA}(\mathbf{k}, \omega) + G^D_{BB}(\mathbf{k}, \omega)]. \quad (7)$$

In Fig. 2 we present an intensity plot of the spectral function for three values of the perpendicular momentum and two impurity concentrations. In Fig. 3 we show four constant $\mathbf{k}$ cuts. It is clear that disorder leads to broad peaks and that the high-energy branch is less affected by the disorder than the low-energy branch. Electron-electron interactions lead to an extra contribution to the self-energy (not included in the plots) that scales linearly with frequency [13], $\mathrm{Im}\Sigma_{ee}(\omega) \propto |\omega|$. Hence, disorder leads to a quasiparticle damping that increases at low frequencies, while the electron-electron contribution increases at high frequencies, the final result is a quasiparticle decay rate that has a *minimum* at a finite frequency. This highly unusual behavior was also found in the case of single layer graphene [10] and is present in *all* multilayer systems. Notice also that the peak positions are shifted by disorder. Another interesting feature is the appearance of a new peak in the spectrum near $k_\perp d = \pi/2$, which is clearly visible in Fig. 3(c) for $n_i = 10^{-3}$. This extra peak is due to the fact that the real part of the self-energies can act as a "mass" term in the Dirac equation leading to the formation of a "pseudogap". For even higher values of the disorder the peak goes away and only a broad shoulder remains.

Transport properties.—The conductivity can be computed from the Kubo formula:

$$\sigma(\omega) = \int dt e^{i\omega t}\langle[J(t), J(0)]\rangle/(S\omega) = i\Pi(\omega)/(\omega + i\delta), \quad (8)$$

where J is appropriate the current operator, and $\Pi(\omega)$ the associated current-current correlation function. The current operators are dictated by gauge invariance [14] and are computed using the Peierls substitution. For instance, for plane 1 with the current in the x direction we find: $J_{x1} = ev_F\sum_{\mathbf{k}}[c^\dagger_{A_1,\mathbf{k}}c_{B_1,\mathbf{k}} + c^\dagger_{B_1,\mathbf{k}}c_{A_1,\mathbf{k}}]$; for the multilayer, the c-axis current operator is $J_\perp = -2et_\perp d\sum_{\mathbf{k}}\sin(k_\perp)\times[c^\dagger_{A_1,\mathbf{k}}c_{A_2,\mathbf{k}} + c^\dagger_{A_2,\mathbf{k}}c_{A_1,\mathbf{k}}]$. We evaluate the current-current correlators with the disorder-averages propagators in the Matsubara formalism [15]. For the real part of the frequency-dependent conductivity we find

$$\mathrm{Re}[\sigma(\omega)]/\sigma_0 = \int d\epsilon[n_F(\omega) - n_F(\omega + \epsilon)]\Xi(\epsilon, \epsilon + \omega)/\omega, \quad (9)$$

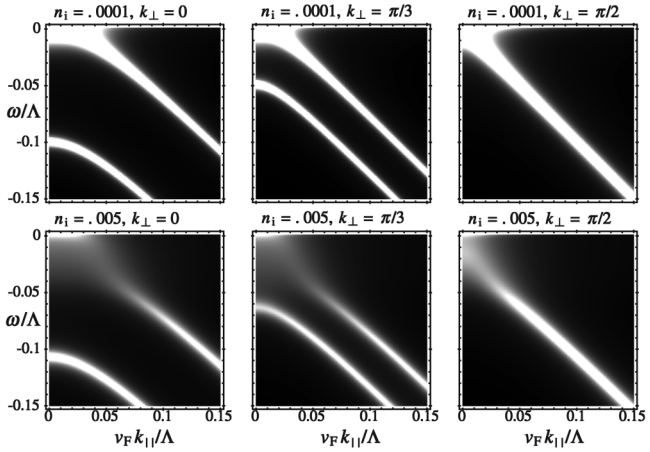

FIG. 2. Intensity plot of the multilayer spectral function (7) in the ω (in units of Λ) versus in-plane momentum $k_\parallel$ (in units of Λ/v_F) plane, for different values of the transverse momentum $k_\perp$ (in units of $1/d$) and impurity concentration. Upper row: $n_i = 10^{-4}$; lower row: $n_i = 5\times10^{-3}$.

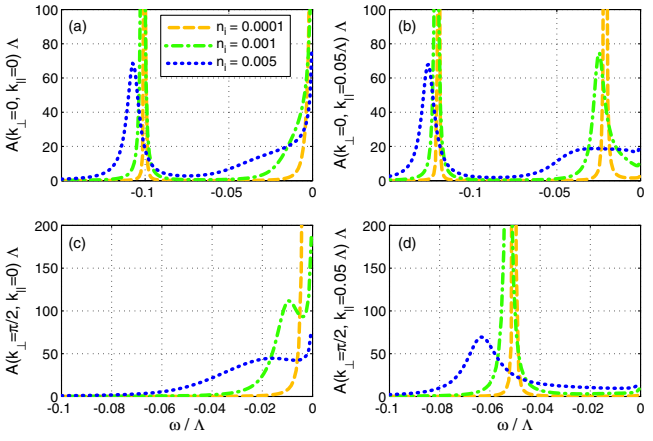

FIG. 3 (color online). Constant $\mathbf{k}$ cuts of the spectral function in the multilayer as a function of the frequency (in units of Λ). (a) $k_\perp = 0$, $k_\parallel = 0$, (b) $k_\perp = 0$, $k_\parallel = 0.05\Lambda$, (c) $k_\perp = \pi/2$, $k_\parallel = 0$, (d) $k_\perp = \pi/2$, $k_\parallel = 0.05\Lambda$.

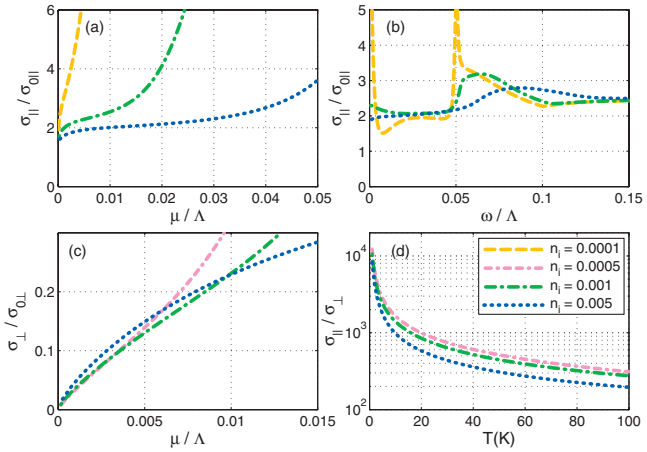

FIG. 4 (color online). (a) In-plane dc conductivity in the bilayer as a function of the chemical potential (in units of Λ). (b) In-plane conductivity in the bilayer as a function of frequency at $T = 300$ K and $\mu = 0$ (in units of Λ). (c) Perpendicular dc conductivity in the multilayer as a function of the chemical potential (in units of Λ). (d) Semilog plot of the transport anisotropy ($\sigma_\parallel/\sigma_\perp$) in the multilayer as a function of the temperature T (in K) at $\mu = 0$.

where $n_F(\epsilon)$ is the Fermi-Dirac function, σ_0 is the unit of conductance [$\sigma_{0\parallel} = 4e^2/\pi h$ for the bilayer, and $\sigma_{0\parallel} = \sigma_{0\perp}(v_F/2t_\perp d)^2$ for the multilayer], Ξ is a kernel that we have evaluated [12]. Note that since we model the impurities as purely local, there are no vertex corrections. We present some of our results in Fig. 4.

The dc conductivities are given by $\sigma_{\rm dc} = \sigma_0 \Xi(\mu, \mu)$, where μ is the chemical potential. In the bilayer

$$\Xi_{\rm dc\parallel} = 2\int_0^{\Lambda^2} d(v_F^2 k^2)\{{\rm Im}[G^D_{AA}(\mu, \mathbf{k})]{\rm Im}[G^D_{BB}(\mu, \mathbf{k})] + {\rm Im}[G_{A_1B_2}(\mu, \mathbf{k})]{\rm Im}[G_{A_2B_1}(\mu, \mathbf{k})]\}. \quad (10)$$

Upon taking the limit $\mu \to 0$, using the asymptotic expressions for the self-energies in Eq. (6), the off-diagonal propagators drop out and the in-plane dc conductivity per plane acquires a universal minimum value given by

$$\sigma_{\parallel,\rm min} = (3/\pi)(e^2/h), \quad (11)$$

independent of the impurity concentration. Hence, as in the case of the single layer [10], we find a universal conductivity minimum albeit with a different value [in the single layer one finds $\sigma_{\rm min} = (4/\pi)(e^2/h)$]. This result shows that in these systems the in-plane conductivity is always of order e^2/h per plane and disorder independent.

The frequency dependence of the conductivity in the bilayer shows some structure. For the cleaner systems a Drude-like peak appears at $\omega = 0$ due to thermally excited carriers. The second peak at $\omega = t_\perp$ is due to interband transitions. The perpendicular transport in the multilayer has the amazing property that close enough to half filling the transport is enhanced by disorder, as can be seen in Fig. 4(c). Also, as one can clearly see in Fig. 4(d), the anisotropy ratio becomes very large as the Dirac point is approached, and the cleaner the system the larger the anisotropy. Using a similar asymptotic expression as in Eq. (6) one expects that the anisotropy diverges as $T^{-2/3}$ exactly at the Dirac point. For small, but finite values of the chemical potential, the anisotropy is still enormous but saturates at a finite value at $T = 0$. Notice, however, that at high temperatures electron-phonon scattering (not discussed here) becomes important and can substantially modify the transport.

Conclusions.—In conclusion, we have presented results for the electronic properties of disordered graphene multilayers showing a behavior that is not that of a normal metal. The unconventional behavior includes divergent self-energies near the Dirac point, the vanishing density of states on the A sublattice, the nonintuitive feature that disorder can increase the out-of-plane transport and the high anisotropy of the system near half filling. These properties show that graphene multilayers are a new class of materials with an unusual metallic state [16].

We thank A. Lanzara for sharing Ref. [16] prior to its publication. A. H. C. N. is supported through NSF Grant No. DMR-0343790. N. M. R. P. thanks ESF Science Programme INSTANS 2005–2010 and FCT under the Grant No. POCTI/FIS/58133/2004. F. G. acknowledges funding from MEC (Spain) through Grant No. FIS2005-05478-C02-01, and the European Union Contract No. 12881 (NEST).

[1] K. S. Novoselov *et al.*, Science **306**, 666 (2004).
[2] K. S. Novoselov *et al.*, Nature (London) **438**, 197 (2005).
[3] Y. Zhang *et al.*, Nature (London) **438**, 201 (2005).
[4] C. Berger *et al.*, J. Phys. Chem. **108**, 19 912 (2004).
[5] K. S. Novoselov *et al.*, Nature Phys. **2**, 177 (2006).
[6] E. McCann and V. I. Fal'ko, Phys. Rev. Lett. **96**, 086805 (2006).
[7] J. Nilsson *et al.*, Phys. Rev. B **73**, 214418 (2006).
[8] P. R. Wallace, Phys. Rev. **71**, 622 (1947).
[9] N. B. Brandt, S. M. Chudinov, and Y. G. Ponomarev, in *Modern Problems in Condensed Matter Sciences*, edited by V. M. Agranovich and A. A. Maradudin (North-Holland, Amsterdam, 1988), Vol. 20.1.
[10] N. M. R. Peres *et al.*, Phys. Rev. B **73**, 125411 (2006).
[11] P. Soven, Phys. Rev. **156**, 809 (1967).
[12] J. Nilsson *et al.* (unpublished).
[13] J. Gonźalez *et al.*, Phys. Rev. Lett. **69**, 172 (1992).
[14] I. Paul and G. Kotliar, Phys. Rev. B **67**, 115131 (2003).
[15] G. D. Mahan, *Many-Particle Physics* (Plenum, New York, 2000).
[16] After the completion of this work, we became aware of recent ARPES data in crystalline graphite that supports our results: S. Y. Zhou *et al.* Nature Phys. **2**, 595 (2006).